2010 IEEE International Conference on Robotics and Automation
Anchorage Convention District
May 3-8, 2010, Anchorage, Alaska, USA

Consistency of the monocular EKF-SLAM algorithm for three different landmark parametrizations

Joan Solà
University of Toulouse, LAAS-CNRS, France. jsola@laas.fr

Abstract— **We benchmark in this article three different landmark parametrizations in monocular 6DOF EKF-SLAM. These parametrizations are *homogeneous points* (HP), *inverse-distance points* (IDP, better known as *inverse-depth*), and the new *anchored homogeneous points* (AHP). The discourse used for describing them is chosen to highlight their differences and similarities, showing that they are just incremental variations of ones with respect to the others. We show for the first time a complete comparison of HP against IDP, two methods that are getting popular, and introduce also for the first time AHP, whose description falls precisely between the other two. The benchmarking is done by running all algorithms on the same data and by using the well-established NEES consistency analysis. Our conclusion is that the new AHP parametrization is the most interesting one for monocular EKF-SLAM (followed by IDP and then HP) because it greatly postpones the apparition of EKF inconsistency.**

I. Introduction

Monocular simultaneous localization and mapping (SLAM) gained popularity back in 2003 thanks to a real-time implementation due to Davison [1]. Davison's technique elegantly solved a great number of problems, but one still remained that occupied researchers on visual SLAM for some years: the problem of landmark initialization. Monocular EKF-SLAM reached maturity with the advent of undelayed initialization techniques, a need firstly stated in 2005 by Solà *et al.* [2], with a preliminary solution based on a previous work in 2004 by Kwok *et al.* [3], and finally solved in 2006 with the inverse-depth landmark parametrization (IDP) due to Montiel *et al.* [4].

The problem of undelayed landmark initialization within monocular EKF-SLAM knows today two main solutions, both of them relying on astute landmark parametrizations: *inverse-distance points* (IDP, better known as inverse-depth, [4], [5]), and *homogeneous points* (HP, used in [6] with a robocentric [14] slgorithm). These parametrizations simultaneously fulfill two key objectives: the ability to encode uncertainty up to infinity with one single Gaussian, and the quasi-linearity of the observation functions within all this uncertainty range. These two assets contribute to make undelayed initialization successful with the use of a simple EKF.

Other authors investigated the possibilities of using different estimation techniques. We have seen IDP used in FastSLAM2.0 [7] and UKF [8], [9] frameworks; and methods based on bundle adjustment [10], [11] or on graph theory [12]. These works are often motivated by inconsistency problems and computational burden associated with EKF-SLAM. However, two aspects keep the classical, EKF solution alive: its simplicity of implementation and the fact that EKF-SLAM is now solved using multi-map techniques. In multi-map systems, each map is of limited size and this naturally renders the computational complexity constant while keeping the inconsistency problems due to non-linearity under reasonable limits.

The consistency issues of EKF-SLAM are well known and have been the subject of numerous studies in the last years. Castellanos *et al.* showed in [13] that inconsistency appears even before the computational burden of the problem becomes prohibitive, and proposed in [14] robocentric SLAM where the local operation of the filter allows for significant linearity improvements. A more concise study of inconsistency was performed by Bailey [15], where the normalized estimation error squared (NEES) is averaged along a number of conditionally independent Monte Carlo runs. This work also shows that using ground-truth Jacobians guarantees filter consistency, and thus that inconsistency comes from the unavoidable errors produced when linearizing the system. Further insights have been provided by Huang *et al.* [16]. Huang shows that the observable subspace of the linearized system is of higher dimension than that of the actual, non-linear one, leading to covariance reductions in directions of the state where no information is available, which is a primary cause of inconsistency. All these studies assumed range-and-bearing sensing and Euclidean landmark parametrizations, exactly as they appear in the original EKF-SLAM solution.

Our case of study is different in two aspects. The first one is that we are dealing with monocular observations that convey partial (bearing-only) information about the landmark locations. The second one, which is a consequence of the first, is that landmark parametrization is no longer the trivial, minimal, Euclidean one, but something more or less complicated that seeks precisely an improvement of linearity. The aim of this paper, however, is not a detailed mathematical analysis but a performance comparison in view of evaluating the impact that landmark parametrization has on filter consistency. We compare three different cases: *inverse-depth points* (IDP), *homogeneous points* (HP), and a new parametrization, *anchored homogeneous points* (AHP). We also aim at highlighting the similarities between them: we show that AHP is just an anchored version of HP, and that IDP is just a lightened version of AHP. Once these relations are established, the different methods are benchmarked: this allows the reader to correlate the results with the theoretical links presented. The benchmarking is performed with Monte-

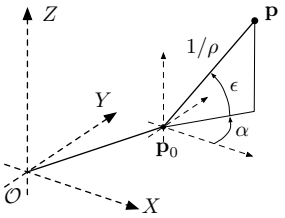

(a) Inverse-distance point (IDP). The anchor point $\mathbf{p}_0$ corresponds to the optical center at initialization time. We encode the unmeasured distance with its inverse ρ.

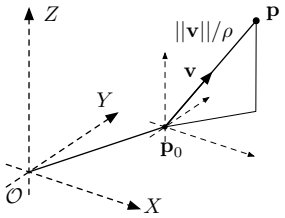

(b) Anchored homogeneous point (AHP). The ray's direction is defined by a vector $\mathbf{v}$ that, together with the inverse distance ρ, constitutes a homogeneous point referenced at the anchor point $\mathbf{p}_0$. There is no need for $\mathbf{v}$ to be a unit vector.

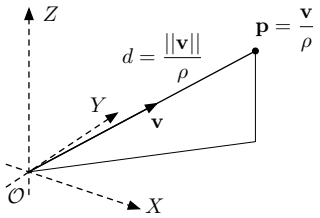

(c) Homogeneous point (HP). The homogeneous part of an AHP is anchored at the origin, and the anchor suppressed.

Fig. 1. The three landmark parametrizations studied in this paper.

Carlo simulations, using the well-established NEES measure [15] to evaluate consistency. We show how inconsistency comes from covariance over-estimation rather than error magnitude, which corroborates Huang's conclusions. The outcome of this evaluation shows that AHP is the best parametrization in terms of filter consistency, clearly outperforming IDP, and that HP is the worst one. Therefore, an important contribution of this paper is the new AHP parametrization.

The rest of this article is organized as follows. We detail in Section II the three landmark parametrizations, with their transformation, and perspective projection and back-projection functions. We describe in Section III the initialization and update mechanisms, valid for all parametrizations. In Section IV we detail the conditions and give the results of the Monte-Carlo consistency analysis, and conclude in Section V with a discussion.

II. Landmark parametrizations

A. Euclidean points (EP)

A Euclidean point $\mathbf{p}$ is trivially coded with three Cartesian coordinates

$$\mathcal{P}_{\mathbb{E}} = \mathbf{p} = \begin{bmatrix} X & Y & Z \end{bmatrix}^\top \in \mathbb{R}^3$$

Transformation to camera frame and pin-hole projection operations resume to

$$\underline{\mathbf{u}} = \mathbf{K}\mathsf{R}^\top(\mathbf{p} - \mathsf{T}) \in \mathbb{P}^2, \tag{1}$$

where $\mathbf{K}$ is the intrinsic matrix, underlined fonts $\underline{\bullet}$ indicate homogeneous coordinates, $\mathsf{R} = \mathsf{R}(\mathsf{Q})$ and T are the rotation matrix and the translation vector defining the camera frame $\mathcal{C} = (\mathsf{T}, \mathsf{Q})$, and Q is a suitable orientation representation (we use quaternions).

Euclidean points lead to severely non-linear observation functions in bearings-only systems and are not suited for undelayed initialization, as it has been extensively demonstrated [2], [3], [6], [7], [17] and most particularly [5]. The parametrizations that follow mitigate this problem and can be used for undelayed initialization with just a few precautions.

B. Inverse-distance points (IDP)

An "inverse-distance" point[1] (IDP, Fig. 1(a)) [5] is coded by a 6-vector containing the Euclidean optical center at initialization time, $\mathbf{p}_0 = (x_0, y_0, z_0)$, elevation and azimuth angles defining the direction of the initial optical ray, (ε, α), and the inverse of the Euclidean distance from $\mathbf{p}_0$ to the 3D point $\mathbf{p}$, denoted by ρ:

$$\begin{aligned} \mathcal{P}_{\mathbb{ID}} &= \begin{bmatrix} \mathbf{p}_0^\top & \varepsilon & \alpha & \rho \end{bmatrix}^\top \\ &= \begin{bmatrix} x_0 & y_0 & z_0 & \varepsilon & \alpha & \rho \end{bmatrix}^\top \in \mathbb{R}^6 \end{aligned} \tag{2}$$

We will refer to the initial optical center $\mathbf{p}_0$ as the *anchor point* of the landmark. An IDP refers to the following EP:

$$\mathbf{p} = \mathbf{p}_0 + \mathbf{v}^*(\varepsilon, \alpha)/\rho \tag{3}$$

where $\mathbf{v}^*(\varepsilon, \alpha)$ is a unit vector in the direction of (ε, α),

$$\mathbf{v}^*(\varepsilon, \alpha) = \begin{bmatrix} \cos(\varepsilon)\cos(\alpha) & \cos(\varepsilon)\sin(\alpha) & \sin(\varepsilon) \end{bmatrix}^\top. \tag{4}$$

Transformation to camera frame and pin-hole projection operations resume to

$$\underline{\mathbf{u}} = \mathbf{K}\mathsf{R}^\top\big(\mathbf{v}^*(\varepsilon, \alpha) - \rho(\mathsf{T} - \mathbf{p}_0)\big). \tag{5}$$

The back-projection and transformation composition necessary for initialization is performed with

$$\mathcal{P}_{\mathbb{ID}} = \begin{bmatrix} \mathbf{p}_0 \\ (\varepsilon, \alpha) \\ \rho \end{bmatrix} = \begin{bmatrix} \mathsf{T} \\ \upsilon^*(\mathsf{R}\mathbf{K}^{-1}\underline{\mathbf{u}}) \\ \rho^{\mathcal{C}} \end{bmatrix}, \tag{6}$$

where $\upsilon^*(\mathbf{v})$ gives elevation and azimuth angles (ε, α) of a director vector $\mathbf{v} = (u, v, w)$,

$$\begin{bmatrix} \varepsilon \\ \alpha \end{bmatrix} = \upsilon^*(u, v, w) = \begin{bmatrix} \arctan(w/\sqrt{u^2 + v^2}) \\ \arctan(v/u) \end{bmatrix}. \tag{7}$$

The inverse-distance parameter $\rho^{\mathcal{C}}$ is defined in the camera frame at initialization time. It must be provided as prior.

[1] In this article we will refer to the originally named "inverse depth" points as *inverse-distance* points, and will use the invariant abbreviation IDP.

TABLE I

SUMMARY OF LANDMARK PARAMETRIZATIONS AND THEIR MAIN MANIPULATIONS

Lmk	parameters	size	transformation	projection	transformation + projection $h()$	back-projection + transf. $g()$
EP	$\mathcal{P}_{\mathbb{E}} = \mathbf{p}$	3	$\mathbf{p} = \mathsf{R}\mathbf{p}^{\mathcal{C}} + \mathsf{T}$	$\underline{\mathbf{u}} = \mathbf{K}\mathbf{p}^{\mathcal{C}}$	$\underline{\mathbf{u}} = \mathbf{K}\mathsf{R}^{\top}(\mathbf{p} - \mathsf{T})$	$\mathbf{p} = t\mathsf{R}\mathbf{K}^{-1}\underline{\mathbf{u}} + \mathsf{T}$
HP	$\mathcal{P}_{\mathbb{H}} = \underline{\mathbf{p}} = (\mathbf{v}, \rho)$	4	$\underline{\mathbf{p}} = \mathbf{H}\underline{\mathbf{p}}^{\mathcal{C}}$	$\underline{\mathbf{u}} = \mathbf{K}\mathbf{v}^{\mathcal{C}}$	$\underline{\mathbf{u}} = \mathbf{K}\mathsf{R}^{\top}(\mathbf{v} - \rho\mathsf{T})$	$\mathcal{P}_{\mathbb{H}} = \underline{\mathbf{p}} = \mathbf{H}\begin{bmatrix}\mathbf{K}^{-1}\underline{\mathbf{u}} \\ \rho^{\mathcal{C}}\end{bmatrix}$
AHP	$\mathcal{P}_{\mathbb{AH}} = (\mathbf{p}_0, \mathbf{v}, \rho)$	7			$\underline{\mathbf{u}} = \mathbf{K}\mathsf{R}^{\top}\big(\mathbf{v} - \rho(\mathsf{T} - \mathbf{p}_0)\big)$	$\mathcal{P}_{\mathbb{AH}} = \begin{bmatrix}\mathsf{T} \\ \mathsf{R}\mathbf{K}^{-1}\underline{\mathbf{u}} \\ \rho^{\mathcal{C}}\end{bmatrix}$
IDP	$\mathcal{P}_{\mathbb{ID}} = (\mathbf{p}_0, \varepsilon, \alpha, \rho)$	6			$\underline{\mathbf{u}} = \mathbf{K}\mathsf{R}^{\top}\big(\mathbf{v}^* - \rho(\mathsf{T} - \mathbf{p}_0)\big)$	$\mathcal{P}_{\mathbb{ID}} = \begin{bmatrix}\mathsf{T} \\ \upsilon^*(\mathsf{R}\mathbf{K}^{-1}\underline{\mathbf{u}}) \\ \rho^{\mathcal{C}}\end{bmatrix}$

C. Anchored homogeneous points (AHP)

IDP points can be parametrized somewhat differently by encoding the optical ray's direction with a vector $\mathbf{v} = (u, v, w)$, avoiding the need for the non-linear transformations (4) and (7). When this vector is unitary, appending the inverse of the distance ρ to it results in a homogeneous point $(u, v, w, \rho) \in \mathbb{P}^3$. This leads to the anchored homogeneous point (AHP, Fig. 1(b)), parametrized with the 7-vector

$$\begin{aligned}\mathcal{P}_{\mathbb{AH}} &= \begin{bmatrix}\mathbf{p}_0^{\top} & \mathbf{v}^{\top} & \rho\end{bmatrix}^{\top} \\ &= \begin{bmatrix}x_0 & y_0 & z_0 & u & v & w & \rho\end{bmatrix}^{\top} \in \mathbb{R}^7\end{aligned} \tag{8}$$

It is worth noticing that a homogeneous point $(\mathbf{v}, \rho)$ does not require $\mathbf{v}$ to be a unit vector. If it is not, the parametrization is absolutely valid but ρ is then not the inverse distance $1/d$ but something proportional to it, *i.e.*, $\rho = \|\mathbf{v}\|/d$.

An AHP refers to the following EP:

$$\mathbf{p} = \mathbf{p}_0 + \mathbf{v}/\rho. \tag{9}$$

Transformation to camera frame and projection resume to

$$\underline{\mathbf{u}} = \mathbf{K}\mathsf{R}^{\top}\big(\mathbf{v} - \rho(\mathsf{T} - \mathbf{p}_0)\big) \in \mathbb{P}^2. \tag{10}$$

The back-projection and transformation composition is done with

$$\mathcal{P}_{\mathbb{AH}} = \begin{bmatrix}\mathbf{p}_0 \\ \mathbf{v} \\ \rho\end{bmatrix} = \begin{bmatrix}\mathsf{T} \\ \mathsf{R}\mathbf{K}^{-1}\underline{\mathbf{u}} \\ \rho^{\mathcal{C}}\end{bmatrix}, \tag{11}$$

where $\rho^{\mathcal{C}}$ must be provided as prior; its relation to distance d is given by $\rho^{\mathcal{C}} = \|\mathbf{K}^{-1}\underline{\mathbf{u}}\|/d$.

D. Homogeneous points (HP)

Homogeneous points have the interesting property of presenting a bi-linear transformation equation:

$$\underline{\mathbf{p}} = \mathbf{H}\underline{\mathbf{p}}^{\mathcal{C}} \triangleq \begin{bmatrix}\mathsf{R}(\mathsf{Q}) & \mathsf{T} \\ 0 & 1\end{bmatrix}\underline{\mathbf{p}}^{\mathcal{C}}. \tag{12}$$

When the uncertainties on the camera position $\mathcal{C} = (\mathsf{T}, \mathsf{Q})$ are small, we can consider the motion matrix $\mathbf{H}$ to be deterministic, and therefore (12) to be exactly linear. In this case Gaussian uncertainties are transformed exactly, so it does not matter where our landmarks are anchored at. We are free to re-anchor the AHP (8) at the origin with

$$\begin{bmatrix}\mathbf{v} \\ \rho\end{bmatrix} \leftarrow \begin{bmatrix}\mathbf{I}_{3\times3} & \mathbf{p}_0 \\ \mathbf{0}_{\mathbf{1}\times\mathbf{3}} & 1\end{bmatrix}\begin{bmatrix}\mathbf{v} \\ \rho\end{bmatrix}, \tag{13}$$

which allows us to remove the anchor $\mathbf{p}_0$. This leads to a purely homogeneous point (HP, Fig. 1(c)), which has already been studied in [6]:

$$\mathcal{P}_{\mathbb{H}} = \begin{bmatrix}\mathbf{v}^{\top} & \rho\end{bmatrix}^{\top} = \begin{bmatrix}u & v & w & \rho\end{bmatrix}^{\top} \in \mathbb{R}^4. \tag{14}$$

A HP refers to the following EP:

$$\mathbf{p} = \mathbf{v}/\rho. \tag{15}$$

Transformation to camera frame and projection resume to

$$\underline{\mathbf{u}} = \mathbf{K}\mathsf{R}^{\top}(\mathbf{v} - \rho\mathsf{T}) \in \mathbb{P}^2. \tag{16}$$

The back-projection and transformation composition is done with

$$\mathcal{P}_{\mathbb{H}} = \underline{\mathbf{p}} = \begin{bmatrix}\mathbf{v} \\ \rho\end{bmatrix} = \mathbf{H}\begin{bmatrix}\mathbf{K}^{-1}\underline{\mathbf{u}} \\ \rho^{\mathcal{C}}\end{bmatrix}, \tag{17}$$

where $\rho^{\mathcal{C}}$ must be provided as prior; its relation to initial distance $d^{\mathcal{C}}$ is given by $\rho^{\mathcal{C}} = \|\mathbf{K}^{-1}\underline{\mathbf{u}}\|/d^{\mathcal{C}}$. Once transformed to the global frame with $\mathbf{H}$, this meaning of $\rho^{\mathcal{C}}$ is lost and therefore not valid for ρ.

E. Final comment

We have presented three parametrizations and shown the links between them. We have chosen to start by IDP purely because of chronological reasons. The reader should be able to construct a discourse in the inverse order: start by HP, well known for their interesting properties in vision, then AHP as an anchored version of HP, then IDP as a lightened version of AHP. We summarize in Table I all parametrizations with their main manipulation expressions. This should help building a coherent picture of the parametrizations suited for monocular EKF-SLAM.

III. INITIALIZATION AND UPDATES

A. Initialization

Undelayed landmark initialization in EKF-SLAM with partial measurements (such as monocular measurements) mimics the algorithm for full measurements and incorporates the non-measured magnitudes as priors:

1) Identify the known magnitudes: measurement $\mathbf{u} \sim \mathcal{N}\{\mathbf{y}, \mathbf{R}\}$ and map $X \sim \mathcal{N}\{\bar{X}, \mathbf{P}\}$, where

$$X = \begin{bmatrix}\mathcal{C} \\ \mathcal{M}\end{bmatrix}, \quad \bar{X} = \begin{bmatrix}\bar{\mathcal{C}} \\ \bar{\mathcal{M}}\end{bmatrix}, \quad \mathbf{P} = \begin{bmatrix}\mathbf{P}_{\mathcal{C}\mathcal{C}} & \mathbf{P}_{\mathcal{C}\mathcal{M}} \\ \mathbf{P}_{\mathcal{M}\mathcal{C}} & \mathbf{P}_{\mathcal{M}\mathcal{M}}\end{bmatrix},$$

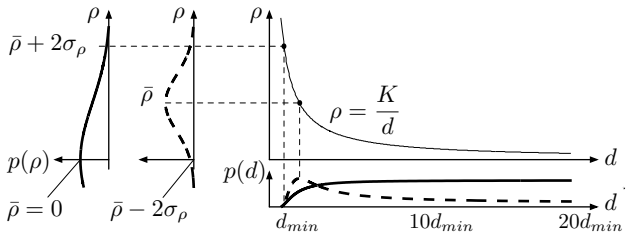

Fig. 2. Inverse-distance PDF. A Gaussian $p(\rho)=\mathcal{N}(\rho-\bar{\rho},\sigma_\rho^2)$ is defined in inverse-distance (vertical axes). We have ample choice: in one extreme (dashed) we may define it so that $\bar{\rho}-2\sigma_\rho=0$; the other extreme (solid) takes $\bar{\rho}=0$. In all cases, we have $(\bar{\rho}+2\sigma_\rho)=K/d_{min}$. They result in PDFs in distance (bottom) that cover from a minimal distance d_{min} to infinity. K is just a proportionality constant, *e.g.* $K=1$ for IDP, and $K=\|\mathbf{K}^{-1}\underline{\mathbf{u}}\|$ for AHP and HP. We can also normalize $\mathbf{K}^{-1}\underline{\mathbf{u}}$ at initialization time and take $K=1$, in which case ρ is exactly equal to inverse-distance.

with $\mathcal{C}=(\mathsf{T},\mathsf{Q})$ the camera frame and $\mathcal{M}$ the set of mapped landmarks.

2) Define a Gaussian prior for the non-measured inverse distance, $\rho^{\mathcal{C}}\sim\mathcal{N}\{\bar{\rho}^{\mathcal{C}},\sigma^2_{\rho^{\mathcal{C}}}\}$, see Fig. 2.
3) Back-project the Gaussian measurement; get landmark mean and Jacobians

$$\bar{\mathcal{P}} = g(\bar{\mathcal{C}},\mathbf{y},\bar{\rho}^{\mathcal{C}})$$
$$\mathbf{G}_{\mathcal{C}} = \left.\frac{dg}{d\mathcal{C}}\right|_{\bar{\mathcal{C}},\mathbf{y},\bar{\rho}^{\mathcal{C}}},\ \mathbf{G}_{\mathbf{u}} = \left.\frac{dg}{d\mathbf{u}}\right|_{\bar{\mathcal{C}},\mathbf{y},\bar{\rho}^{\mathcal{C}}},\ \mathbf{G}_{\rho} = \left.\frac{dg}{d\rho}\right|_{\bar{\mathcal{C}},\mathbf{y},\bar{\rho}^{\mathcal{C}}}$$

with $g(\mathcal{C},\mathbf{u},\rho^{\mathcal{C}})$ one of the back-projection functions in Table I, $\mathcal{C}=(\mathsf{T},\mathsf{Q})$, $\mathsf{R}=\mathsf{R}(\mathsf{Q})$ and $\underline{\mathbf{u}}=[\mathbf{u}^\top\ 1]^\top$.

4) Compute landmark co- and cross-variances

$$\mathbf{P}_{\mathcal{P}\mathcal{P}} = \mathbf{G}_{\mathcal{C}}\mathbf{P}_{\mathcal{C}\mathcal{C}}\mathbf{G}_{\mathcal{C}}^\top + \mathbf{G}_{\mathbf{u}}\mathbf{R}\mathbf{G}_{\mathbf{u}}^\top + \mathbf{G}_{\rho}\sigma^2_{\rho^{\mathcal{C}}}\mathbf{G}_{\rho}^\top$$
$$\mathbf{P}_{\mathcal{P}X} = \mathbf{G}_{\mathcal{C}}\mathbf{P}_{\mathcal{C}X}$$

with $\mathbf{P}_{\mathcal{C}X}=[\mathbf{P}_{\mathcal{C}\mathcal{C}}\ \mathbf{P}_{\mathcal{C}\mathcal{M}}]$.

5) Augment the SLAM map

$$\bar{X}\leftarrow\begin{bmatrix}\bar{X}\\ \bar{\mathcal{P}}\end{bmatrix},\qquad \mathbf{P}\leftarrow\begin{bmatrix}\mathbf{P} & \mathbf{P}_{\mathcal{P}X}^\top\\ \mathbf{P}_{\mathcal{P}X} & \mathbf{P}_{\mathcal{P}\mathcal{P}}\end{bmatrix}.$$

B. Updates

Updates follow the standard EKF-SLAM formulation. The observation functions $\mathbf{u}=h(\mathcal{C},\mathcal{P})$ are the composition of the ones in Table I with the homogeneous-to-Euclidean transform: if $\underline{\mathbf{u}}=[u,v,w]^\top$ then $\mathbf{u}=[u/w,v/w]^\top$.

IV. Consistency evaluation

We benchmark HP, AHP and IDP for filter consistency using the same simulated scenario, the same software and the same seeds for the random generator. A description of the benchmarking methods and the simulation conditions follows, and results are given at the end of this section.

A. Normalized estimation error squared (NEES)

Here we follow [15]. We analyze filter consistency using the average normalized estimation error squared (NEES). When ground truth about a variable $\mathbf{x}_k$ is known, the NEES of its estimate $\mathcal{N}\{\hat{\mathbf{x}}_k,\mathbf{P}_k\}$ is defined at each time k by

$$\epsilon_k=(\mathbf{x}_k-\hat{\mathbf{x}}_k)^\top\mathbf{P}_k^{-1}(\mathbf{x}_k-\hat{\mathbf{x}}_k). \tag{18}$$

TABLE II
Simulation parameters for all experiments

Concept	Param.	Set 1	Set 2
Pose step	$(\Delta X,\Delta\psi)$	$(8\text{cm},0.9°)$	$(4\text{cm},0.45°)$
Lin. noise	$(\sigma_X,\sigma_Y,\sigma_Z)$	1cm	0.5cm
Ang. noise	$(\sigma_\phi,\sigma_\theta,\sigma_\psi)$	$0.1°$	$0.05°$
Img. size		640×480 pix	
Focal	(α_u,α_v)	320 pix, $HFOV=90°$	
Pix. noise	$\sigma_{\mathbf{u}}$	1 pix	
$\rho^{\mathcal{C}}$ prior	$(\bar{\rho}^{\mathcal{C}},\sigma_{\rho^{\mathcal{C}}})$	$(0.01,0.5)$ m^{-1}	$(0.01,0.5)$ m^{-1}
			$(1.0,1.0)$ m^{-1}

Under the hypothesis of consistent filtering of a linear-Gaussian system, ϵ_k obeys a χ^2 distribution with $\dim(\mathbf{x}_k)$ degrees of freedom (DOF), noted $\chi^2_{\dim(\mathbf{x})}$, whose expectation over an increasing number of runs converges to the state dimension, $\mathbb{E}[\epsilon_k]=\dim(\mathbf{x}_k)$. The linear-Gaussian hypothesis can then be statistically evaluated by means of a χ^2 acceptance test over a set of $N<\infty$ Monte-Carlo runs.

Given N Monte-Carlo runs, $\sum_{i=1}^N\epsilon_{ik}$ obeys a $\chi^2_{N\dim(\mathbf{x})}$ distribution. The bounds of the *double-sided* 95% *probability concentration region* are given by the $\chi^2_{N\dim(\mathbf{x})}$ values corresponding to tail probabilities of 2.5% and 97.5%. For 6-DOF SLAM and $N=25$ runs, we have the lower and upper bounds $\{\underline{\nu};\overline{\nu}\}=\chi^2_{(6\times25)}(1-0.025;1-0.975)=\{117.985;185.800\}$.

The average NEES is computed as

$$\bar{\epsilon}_k\triangleq\frac{1}{N}\sum_{i=1}^N\epsilon_{ik}. \tag{19}$$

We compare the average NEES against $\{\underline{\varepsilon};\overline{\varepsilon}\}=\frac{1}{N}\{\underline{\nu};\overline{\nu}\}=\{4.719;7.432\}$. If the average NEES is below the lower bound for some significant amount of time, the filter is conservative. If it is above the upper bound, the filter is optimistic and therefore inconsistent.

B. Software and SLAM algorithm

We have made available the software used for simulations [18]. It consists in a 6-DOF EKF-SLAM system written in MATLAB®, with simulation and 3D graphics capabilities.

The algorithm is organized as an active-search-based SLAM [19], which allows us to optimize information gain with a limited number of updates per frame. At each frame, we perform updates to the 10 most informative landmarks. We also attempt to initialize one landmark per frame. Inconsistent and unstable landmarks are deleted from the map to avoid map corruption.

C. Simulated scenario

We simulate a robot performing a circular trajectory in an area of $12m\times12m$, populated with 72 landmarks forming a cloister (Fig. 3). The robot receives noisy control inputs which are used for the prediction stage of the EKF, fixing the scale factor. One noisy image per control step is gathered with a single camera heading forward. Two sets of

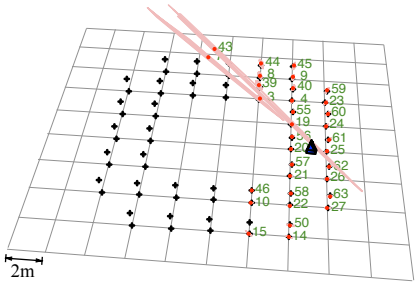

Fig. 3. Simulated 3D environment for 6-DOF monocular SLAM.

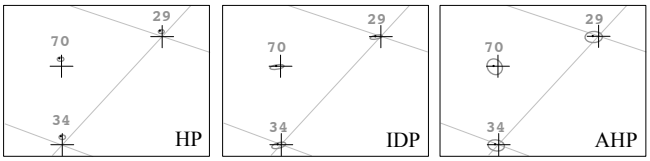

Fig. 4. 3D view of some landmark 3σ estimates at the end of the first loop. In accordance with [16], inconsistency comes from covariance overestimation rather than mean errors. See the accompanying video.

parameters have been used for the tests (the nominal and perturbation levels of all these magnitudes, together with the inverse-distance priors used, are all summarized in Table II). In the first set, the robot makes two turns to the cloister (800 frames are processed). The second set uses smaller odometry increments and perturbations, and the trajectory is limited to one quarter of a turn (200 frames).

D. Results

We provide an accompanying video showing the three methods running in parallel. The differences in behavior are not appreciable in naked eye in the 3D movies, showing that inconsistency is not a matter of larger or smaller absolute errors, but on how accurate the filter thinks their estimates are. We need to zoom in to appreciate incorrect operation (Fig. 4): IDP and HP estimate too small covariances. As a result, the NEES behavior of the three parametrizations is radically different (Fig. 5, please note the logarithmic vertical scale):

- HP behaves poorly. Of the 25 runs, one diverged, and 35 landmarks had to be deleted due to inconsistent observations (22 of which during the divergent run).
- IDP shows better performance but also escapes consistency very quickly. No run diverged but inconsistent observations triggered landmark deletion in two occasions.
- AHP behaves consistently, certainly with a slight tendency to inconsistency, until shortly after the first loop closure. During the second turn the filter is inconsistent but it does not seem to degrade too quickly. No landmarks were declared inconsistent.

We tuned the algorithms with the second set of parameters in order to improve linearity: odometry steps and noise are cut in half, and the filter is bootstrapped with 10 landmarks being initialized at the first frame. Here, we focus on the

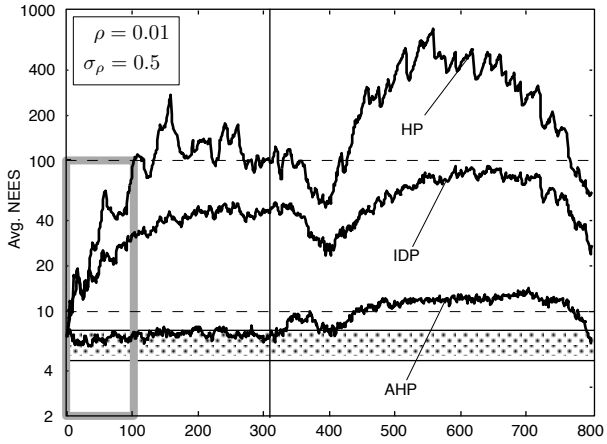

Fig. 5. Consistency of HP, IDP and AHP. Average NEES of the 6-DOF vehicle pose $[x, y, z, \phi, \theta, \psi]^\top$ over 25 runs for 800 frames (2 turns) and parameters of Set 1. The dotted horizontal band between abscissas $\underline{\epsilon} = 4.719$ and $\bar{\epsilon} = 7.432$ marks the 95% consistency region: the filter is inconsistent if the average NEES is above its upper bound. The vertical line marks the loop closure at frame 308. The framed area corresponds to the area covered by Figs. 6 and 7.

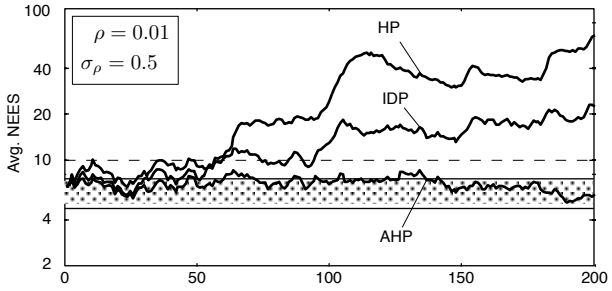

Fig. 6. Average NEES over 25 runs for 200 frames (1/4 turn) with parameters of Set 2 and 10 initializations in the first frame.

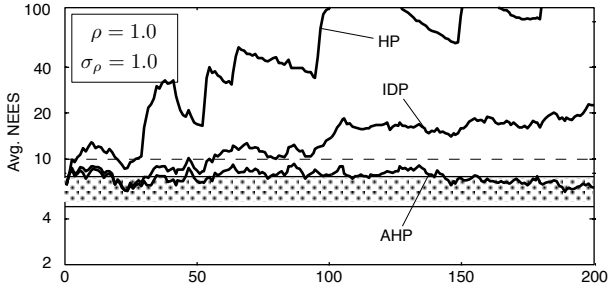

Fig. 7. Average NEES over 25 runs for 200 frames (1/4 turn) with parameters of Set 2 and 10 initializations in the first frame, using an alternative prior $(\bar{\rho}, \sigma_\rho) = (1.0, 1.0)$.

first quarter of the loop to see the moment when the filters loose consistency. The results in Fig. 6 show only a partial improvement with respect to those of Set 1 (these 200 frames correspond to the first 100 frames in Fig. 5): HP is just not good, IDP is better than before but only keeps track until frame 50, and AHP is again the only one to behave consistently.

A third test consisted in selecting a different prior for the unmeasurable inverse-distance. Now we use the couple

$(\bar{\rho}, \sigma_\rho) = (1.0, 1.0)$. By comparing the plots in Fig. 7 against those in Fig. 6 we see that IDP and AHP are virtually insensitive to large variations of these parameters, while the contrary must be said for HP, which degraded even further. It seems, even if for AHP and IDP the difference is small, that the filter behaves better with landmarks initialized at (or close to) infinity (Fig. 6, $\bar{\rho}^{\mathcal{C}} = 0.01\mathrm{m}^{-1}$) than at some close distance (Fig. 7, $\bar{\rho}^{\mathcal{C}} = 1\mathrm{m}^{-1}$).

V. Discussion and conclusion

We are dealing with 3 parametrizations. One is not anchored (HP); the other two are anchored (IDP and AHP). Thanks to the cross-correlations stored in the EKF, the anchor allows the filter to account for accumulated errors only from the anchor to the current position (terms $(\mathsf{T} - \mathbf{p}_0)$ in Table I), not from the origin of coordinates (term T). This is consistent with HP performing clearly worse than IDP and AHP.

Thanks to the superior linearity of homogeneous points with respect to the polar representation of IDP, we expected AHP to be better than IDP. Our experiments showed that the improvement is very significant. We see two reasons for this:

First, the ray direction in AHP is a 3D vector $\mathbf{v}$ that, importantly, is not forced to unity. The fact that its norm can evolve during filtering allows the filter to work more relaxed (there is redundancy over an equivalence class, thus lack of constraints). So when an update occurs, the correction effect can be shared between several dimensions, including of course ρ. In IDP there is no such redundancy and the filter works more "constrained". When it comes to deal with non-linearity, these constraints contribute to larger errors. It is therefore important not to normalize the vector $\mathbf{v}$ at each frame.

Second, the transformation equations in AHP are more linear than those in IDP, because in IDP we have the trigonometric functions (4) and (7). In fact, AHP only differs from IDP in two single lines of code: those performing such equations. This point should be, we feel, only of relative importance, because these angles are well observed from the first observation and therefore the trigonometric functions can be considered quite linear inside the uncertainty region, which is small. However, its effect can only contribute to increase linearization errors.

Regarding the increase in computational costs derived from a larger parametrization size (7 instead of 6), we point here that the linearity measure for IDP [5] can be applied to AHP as-is to trigger a reparametrization. Reparametrization to Euclidean has virtually no effect on NEES results (something we did not show here for space reasons), and only a very small degradation can be observed. This degradation is of the order of the one observed when changing the prior values of $\rho^{\mathcal{C}}$, which we saw in Figs. 6 and 7. The gain in computational power, however, largely compensates for it.

Regarding terminology, IDP could be renamed AMPP (*Anchored Modified Polar Point*): it is anchored, and it is in polar coordinates except for the radius which is inverse-radius (therefore the "modified polar"). This would produce a consistent picture, where the concept of "inverse-distance", as we have seen, is shared among all the parametrizations. To complete the picture, we notice that the AMPP's un-anchored counterpart, *Modified Polar Point* (MPP), not presented in this paper, had already been studied in the 80's in the bearing-only tracking literature with similar problematic and justification [20]. Its use in monocular EKF-SLAM is not recommended: it presents a singularity at the origin, and if we draw the correct conclusions from the present paper, it should behave even worse than HP, as it happens to AMPP (*i.e.* IDP) with respect to AHP.

References

[1] A. J. Davison, "Real-time simultaneous localisation and mapping with a single camera," in *Int. Conf. on Computer Vision*, vol. 2, Nice, October 2003, pp. 1403–1410.

[2] J. Solà, A. Monin, M. Devy, and T. Lemaire, "Undelayed initialization in bearing only SLAM," in *IEEE/RSJ Int. Conf. on Intelligent Robots and Systems*, Edmonton, Canada, 2005, pp. 2499–2504.

[3] N. M. Kwok and G. Dissanayake, "An efficient multiple hypothesis filter for bearing-only SLAM," in *IEEE/RSJ Int. Conf. on Intelligent Robots and Systems*, Sendai, Japan, 2004.

[4] J. Montiel, J. Civera, and A. J. Davison, "Unified inverse depth parametrization for monocular SLAM," in *Robotics: Science and Systems*, Philadelphia, USA, August 2006.

[5] J. Civera, A. Davison, and J. Montiel, "Inverse depth parametrization for monocular SLAM," *IEEE Trans. on Robotics*, vol. 24, no. 5, 2008.

[6] D. Marzorati, M. Matteucci, D. Migliore, and D. G. Sorrenti, "Monocular SLAM with inverse scaling parametrization," in *Proc. of the British Machine Vision Conference*, Leeds, 2008.

[7] E. Eade and T. Drummond, "Scalable monocular SLAM," *IEEE Int. Conf. on Computer Vision and Pattern Recognition*, vol. 1, pp. 469–476, 2006.

[8] N. Sunderhauf, S. Lange, and P. Protzel, "Using the unscented kalman filter in mono-SLAM with inverse depth parametrization for autonomous airship control," in *IEEE Int. Workshop on Safety, Security and Rescue Robotics*, Rome, 2007.

[9] S. A. Holmes, G. Klein, and D. W. Murray, "A square root UKF for visual monoSLAM," in *IEEE Int. Conf. on Robotics and Automation*, Pasadena, 2008.

[10] G. Klein and D. Murray, "Parallel tracking and mapping for small AR workspaces," in *Proceedings of the 2007 6th IEEE and ACM International Symposium on Mixed and Augmented Reality*. IEEE Computer Society, 2007, pp. 1–10.

[11] K. Konolige and M. Agrawal, "FrameSLAM: From bundle adjustment to real-time visual mapping," *IEEE Trans. on Robotics*, vol. 24, no. 5, pp. 1066–1077, Oct. 2008.

[12] E. Eade and T. Drummond, "Monocular slam as a graph of coalesced observations," in *IEEE Int. Conf. on Computer Vision*, 2007.

[13] J. A. Castellanos, J. Neira, and J. D. Tardós, "Limits to the consistency of the EKF-based SLAM," in *5th IFAC Symp. on Intelligent Autonomous Vehicles*, Lisboa, PT, July 2004.

[14] J. A. Castellanos, R. Martinez-Cantin, J. Tardós, and J. Neira, "Robocentric map joining: improving the consistency of EKF-SLAM," in *Robotics and Autonomous Systems*, vol. 55, no. 1, 2007, pp. 21–29.

[15] T. Bailey, J. Nieto, J. Guivant, M. Stevens, and E. Nebot, "Consistency of the EKF-SLAM algorithm," in *IEEE/RSJ Int. Conf. on Intelligent Robots and Systems*, Beijing, China, October 2006, pp. 3562–3568.

[16] A. M. G.P. Huang and S. Roumeliotis, "Analysis and improvement of the consistency of extended Kalman filter based SLAM," in *IEEE Int. Conf. on Robotics and Automation*, 2008, pp. 473–479.

[17] T. Bailey, "Constrained initialisation for bearing-only SLAM," in *Int. Conf. on Robotics and Automation*, vol. 2, 2003, pp. 1966–1971.

[18] J. Solà, D. Marquez, J. M. Codol, and T. Vidal-Calleja. (2009) An EKF-SLAM toolbox for MATLAB. [Online]. Available: http://homepages.laas.fr/jsola/JoanSola/eng/toolbox.html

[19] A. J. Davison, I. D. Reid, N. D. Molton, and O. Stasse, "MonoSLAM: Real-time single camera SLAM," *Trans. on Pattern Analysis and Machine Intelligence*, vol. 29, no. 6, pp. 1052–1067, June 2007.

[20] V. Aidala and S. Hammel, "Utilization of modified polar coordinates for bearings-only tracking," *IEEE Transactions on Automatic Control*, vol. 28, no. 3, pp. 283 – 294, March 1983.